

IGR J11014-6103: a newly discovered pulsar wind nebula?

L. Pavan¹, E. Bozzo¹, G. Pühlhofer², C. Ferrigno¹, M. Balbo¹, and R. Walter¹

¹ ISDC data center for astrophysics of the University of Geneva chemin d'Écogia, 16 1290 Versoix Switzerland.

² Institut für Astronomie und Astrophysik, Kepler Center for Astro and Particle Physics, Eberhard-Karls-Universität, Sand 1, 72076 Tübingen, Germany

Received 2011 May 31; accepted 2011 July 09

ABSTRACT

Context. IGR J11014-6103 is one of the still unidentified hard X-ray *INTEGRAL* sources, reported for the first time in the 4th IBIS/ISGRI catalog.

Aims. We investigated the nature of IGR J11014-6103 by carrying out a multiwavelength analysis of the available archival observations performed in the direction of the source.

Methods. We present first the results of the timing and spectral analysis of all the X-ray observations of IGR J11014-6103 carried out with *ROSAT*, *ASCA*, *Einstein*, *Swift*, and *XMM-Newton*, and then use them to search for possible counterparts to the source in the optical, infra-red, radio and γ -ray domain.

Results. Our analysis revealed that IGR J11014-6103 is comprised of three different X-ray emitting regions: a point-like source, an extended object and a cometary-like “tail” (~ 4 arcmin). A possible radio counterpart positionally coincident with the source was also identified.

Conclusions. Based on these results, we suggest that the emission from IGR J11014-6103 is generated by a pulsar wind nebula produced by a high-velocity pulsar. IGR J11014-6103 might be the first of these systems detected with *INTEGRAL* IBIS/ISGRI.

Key words. stars: individual IGR J11014-6103

1. Introduction

The IBIS/ISGRI telescope (Ubertini et al. 2003) onboard *INTEGRAL* (Winkler et al. 2003) has been operating since seven years from now, and the latest available catalog of sources detected with this telescope contains more than 700 objects (Bird et al. 2010). A large fraction of them belongs to the class of X-ray binaries (26%) and active galactic nuclei (35%); a relatively small fraction is represented by cataclysmic variables (5%), and another 4% comprises supernova remnants, globular clusters and soft γ -ray repeaters. About 30% of the IBIS/ISGRI sources are still unclassified (see e.g. Chaty et al. 2010, for a recent review).

In this paper, we investigate the nature of the still unidentified *INTEGRAL* source IGR J11014-6103. This source was reported for the first time in the 4th IBIS/ISGRI catalog (Bird et al. 2010), and was detected in the IBIS/ISGRI mosaic at a significance level of 5.4σ (20-100 keV). The best determined *INTEGRAL* position of IGR J11014-6103 is at $RA=165.341$ deg, $Dec=-61.056$ deg (J2000), with an associated uncertainty of 4.3 arcmin (90% c.l.). The averaged source fluxes in the 20-40 keV and 40-100 keV energy band are 0.4 ± 0.1 mCrab and 0.6 ± 0.2 mCrab, respectively¹. The light curve of the source, obtained from the online tool HEAVENS² (Walter et al. 2010), does not show evidence of variability. A possible counterpart to IGR J11014-6103 in the soft X-ray (0.3-10 keV) domain was identified by Malizia et al. (2011). In the *Swift*/XRT field of

view (FOV) around IGR J11014-6103, they detected a source located at $RA=165.44$ deg, $Dec=-61.022$ deg (associated uncertainty $\sim 6''$). By using the refined X-ray position, these authors also suggested that IGR J11014-6103 could be associated to the *ROSAT* source 1RXHJ110146.1-610121 and the serendipitous *XMM-Newton* source 2XMMJ110147.1-61012.

In Sect. 2 we report on the analysis of all the available X-ray observations performed with *Swift*, *XMM-Newton*, *ROSAT*, and *ASCA*, in the direction of IGR J11014-6103. We use the results of this analysis in Sect. 3 to search for possible counterparts to the source in the optical, infra-red and radio domains. A discussion on the nature of IGR J11014-6103 is presented in Sect. 4.

2. X-ray observations of IGR J11014-6103

A summary of all X-ray observations analyzed in this section is provided in Table 1.

2.1. Swift

The FOV around IGR J11014-6103 was observed twice with *Swift*/XRT on 2011 March 10 and 12 for a total exposure time of 3.1 ks and 2.1 ks, respectively (observations ID. 00045395001 and 00045395002). We analyzed the *Swift*/XRT (Gehrels et al. 2004) data collected in photon counting mode (PC) by using standard procedures (Burrows et al. 2005) and the latest calibration files available. Filtering and screening criteria were applied by using FTOOLS, and only event grades of 0-12 were considered. Exposure maps were created through the XRTEXPOMAP task. No obvious sources were detected in the two observations separately. We maximized the S/N by summing-up all the available data (effective exposure time 5.1 ks) and ex-

Send offprint requests to: lucia.pavan@unige.ch

¹ 1 mCrab corresponds to 7.57×10^{-12} erg cm⁻² s⁻¹ in the 20-40 keV energy band and to 9.42×10^{-12} erg cm⁻² s⁻¹ in the 40-100 keV energy band.

² <http://www.isdc.unige.ch/heavens>

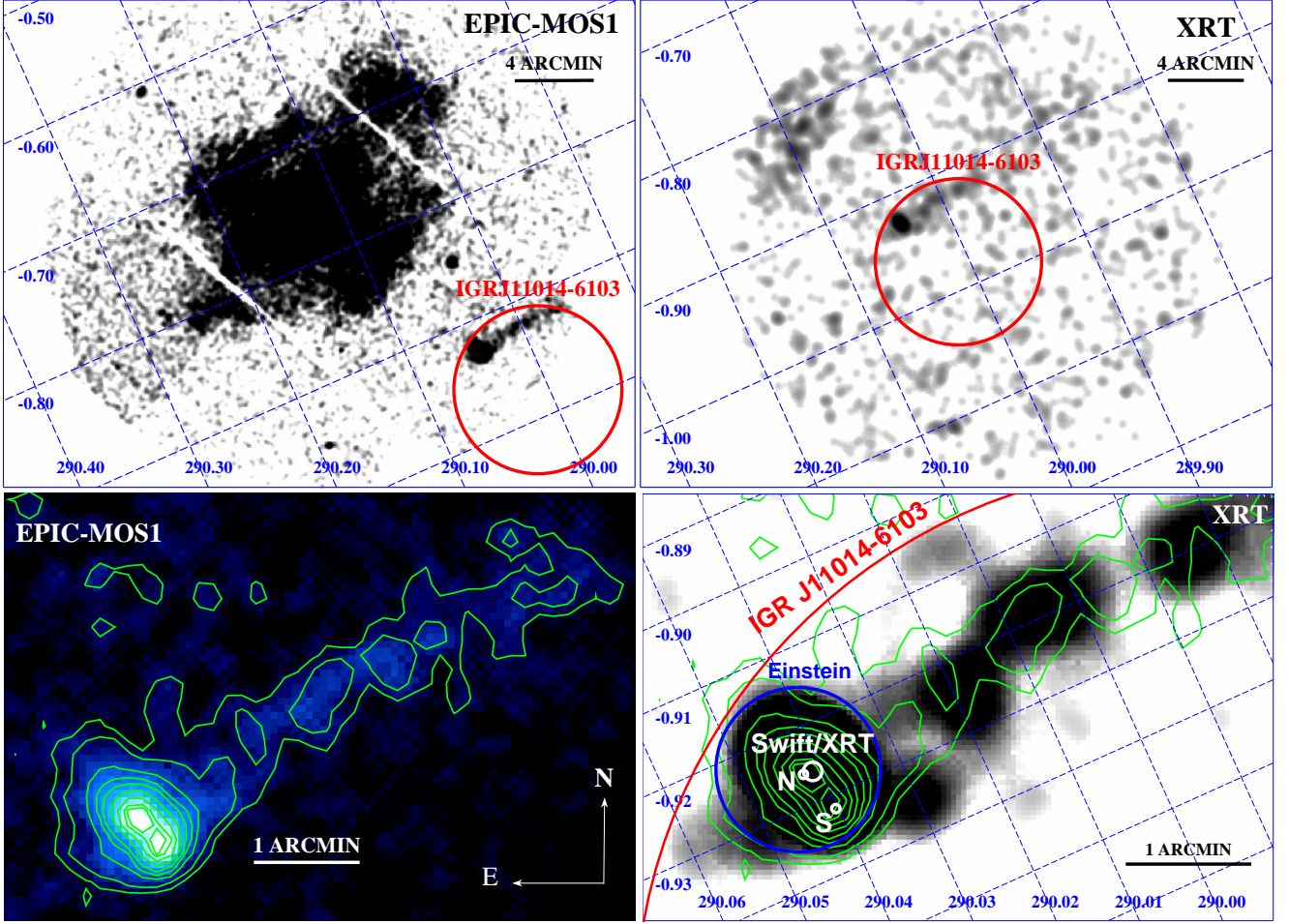


Fig. 1. *Upper left:* FOV around IGR J11014-6103 as observed by EPIC-MOS1 on-board *XMM-Newton* (0.5-12 keV). *Upper right:* *Swift*/XRT FOV around IGR J11014-6103 (1-9 keV). *Bottom left:* zoom of the EPIC-MOS1 FOV. In this case we kept the colours and removed the coordinate grid and the error circles around the detected sources for clarity. *Bottom right:* zoom of the XRT FOV. In this figure we marked the source detected with *Swift* (uncertainty of 4.4'' at 90% c.l.), and sources N and S detected with *XMM-Newton* (uncertainty of 2'' at 90% c.l.). The contours determined from the *XMM-Newton* observations are also overplotted (in green), together with the error circle representing the *INTEGRAL* position of IGR J11014-6103 (in red) and the error circle of the Einstein source 2E 2383 (in blue, uncertainty of 39'' at 90% c.l., see Sect. 2.5). The intensity scale, here and in the following images, is logarithmic and the grid is in galactic coordinates.

Table 1. X-ray observation log of IGR J11014-6103.

Instr	OBS ID	START TIME (MJD)	Exp (ks)
<i>Swift</i>	00045395002	55632	3.1
	00045395001	55630	2.1
<i>XMM-Newton</i>	0152570101	52841	60
	0111210201	51753	11
<i>ROSAT</i>	RH500445A01	50627	46
<i>ASCA</i>	51021010	49733	40
	51021000	49412	43
<i>Einstein</i>	2161	44463	11

tracted a single image of the XRT FOV around IGR J11014-6103. In this image, we detected a faint source ($S/N=5.5$ in the 1-9 keV energy band, see Fig. 1) at the position $RA=165.444$ deg, $Dec=-61.023$ deg (associated uncertainty 4.4'' at 90% c.l.; we used the *XRTCENTROID* tool). This is compatible with being the same source already identified by Malizia et al. (2011), and is

the only source detected inside the *INTEGRAL* error box. It is thus the most likely counterpart to IGR J11014-6103 in soft X-rays. Given the relatively short exposure time and the low count rate of the source, we could not extract a meaningful spectrum. Instead, we estimated the source count rate (0.011 ± 0.002 counts/s, 1-9 keV) with *SOSTA* (available within the *ftool* *XIM-AGE*), and used this result within *WEBPIMMS* in order to derive the corresponding X-ray flux (see also Bozzo et al. 2009). In the conversion between count rate and flux, we adopted an absorbed ($N_H=0.7 \times 10^{22}$ cm $^{-2}$) power law ($\Gamma=1.6$) model (see Sect. 2.2). The inferred X-ray flux in the 2-10 keV energy band was $(6.3 \pm 1.2) \times 10^{-13}$ erg cm $^{-2}$ s $^{-1}$ (not corrected for absorption). Even though a single point source is detected with the *XRTCENTROID* tool, Fig. 1 reveals a marginal evidence for diffuse emission around the source and the presence of an elongated structure (~ 4 arcmin) extending in the north-west direction from the point source. We discuss further these evidences in Sect. 2.2.

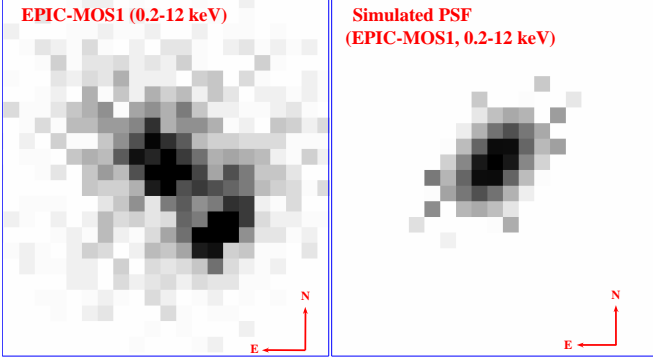


Fig. 2. *Left:* close view of the EPIC-MOS1 FOV around sources N and S (see Sect. 2.2); *Right:* simulated PSF of the EPIC-MOS1 camera at energies in the (0.2-12) keV energy range by assuming the same off-set position as that of sources N and S. The two panels have the same angular scale. The simulated PSF does not show the double peak profile seen in the real data. We also note that the distortion due to the off-set position of the two sources would occur in a different direction with respect to the separation between the two sources.

2.2. XMM-Newton

XMM-Newton observed the region around IGR J11014-6103 on 28 July 2000 (obs. ID 0111210201, total exposure time ~ 11 ksec) and on 21 July 2003 (obs. ID 0152570101, total exposure time ~ 60 ksec). In both cases, the observations were centered on the nearby supernova remnant (SNR) MSH 11-61A, and thus IGR J11014-6103 was off-set with respect to the instrument aim-point by about 15 arcmin. During obs. ID 0152570101, the EPIC-pn and EPIC-MOS cameras were operated in small window and full frame mode, respectively. IGR J11014-6103 was only within the EPIC-MOS FOV. During obs. ID 0111210201 all the EPIC cameras were operated in full frame mode, and IGR J11014-6103 was observed with both the EPIC-pn and EPIC-MOS. In all cases, only part of the *INTEGRAL* error circle around IGR J11014-6103 was included in the FOV of the EPIC cameras (see Fig. 1).

We processed the *XMM-Newton* observation data files with the two pipelines *EPPROC* and *EMPROC* in order to produce EPIC-pn and EPIC-MOS cleaned event files, respectively (SAS v.10.0.1). To identify the high background time intervals, we followed the SAS online analysis thread³ and extracted the lightcurves from the full FOV of the EPIC cameras in the 10-12 keV energy band. We discarded from further analysis the time intervals in which the 10-12 keV FOV count rate was larger than 0.4 cts/s. The resulting effective exposure times were 47.3 ks and 8.0 ks (5.7 ks) for the EPIC-MOS1 (EPIC-pn) cameras in the observation ID 0152570101 and 0111210201, respectively. All cleaned event files were barycentered with the *barycen* tool.

A visual inspection of the EPIC-MOS image extracted from the *XMM-Newton* observation with the longer exposure time (ID 0152570101, see Fig. 1) reveals that the source detected with *Swift*/XRT is indeed composed of three different emitting regions: two sources separated by ~ 22 arcsec (hereafter sources N and S) and a dimmer elongated structure (~ 4 arcmin, hereafter, the “tail”). In the EPIC images extracted from obs. ID 0111210201 only the two brighter sources are clearly visible. In this observation, the tail is only marginally detectable

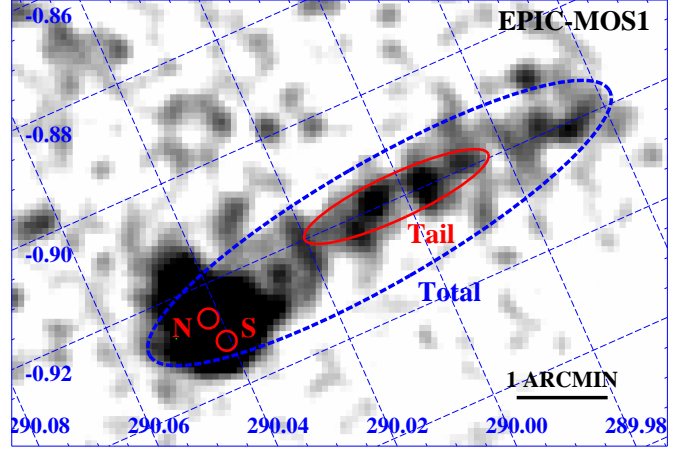


Fig. 3. Zoom of the EPIC-MOS1 FOV around IGR J11014-6103 during observation ID. 0152570101 (0.2-12 keV). The regions used for the extraction of the spectra of sources N and S are indicated with red small circles; the region used for the spectral analysis of the tail with a red ellipse. We also show the extraction region used to perform the spectral analysis of the entire emitting region (dashed ellipse; see Sect. 2.2).

due to the shorter exposure time. In order to check that sources N and S are not just produced by the distortion of the EPIC-MOS point spread function (PSF) at large off-set angles, we simulated with the *psfgen* task the 2D-PSF of the instrument at the location of these two sources. We used a circular region for the simulation ~ 180 arcsec wide centered on source N and set the level parameter to “ELLBETA”. The comparison between the simulated PSF profiles and the measured intensity profiles obtained from the data is shown in Fig. 2. The simulated PSF did not present a double peak in the intensity profile in a direction comparable with that observed from the *XMM-Newton* data. In particular, we note that the distortion of the PSF caused by the off-axis position of the source on the EPIC-MOS detectors occurs preferably along the azimuthal direction, whereas sources N and S are separated in the opposite direction.

Sources N and S were also already identified in the second *XMM-Newton* catalog of serendipitous X-ray sources (Watson et al. 2009) as 2XMM J110147.1-610124 and 2XMM J110145.0-610140, respectively. The best determined positions are ($RA=165.4465$ deg, $Dec=-61.0234$ deg) for the first, and ($RA=165.4377$ deg, $Dec=-61.0279$ deg) for the latter (the nominal positional accuracy of the EPIC cameras is $\sim 2''$, see e.g. Pavan et al. 2011, and references therein). 2XMM J110147.1-610124 is reported as extended, and is characterized by a radial elongation of 8.1 arcsec.

In Fig. 1 the image extracted from *Swift*/XRT is compared with that obtained from the deeper *XMM-Newton* observation. The contours around the extended emission from *XMM-Newton* coincide well with the emission in XRT. This confirms the marginal detection of the extended emission noticed before in the *Swift*/XRT data (see Sect. 2.1), and suggests that the single point source detected with this telescope is indeed a blend of the two brighter objects revealed by *XMM-Newton*.

We also performed a spectral analysis of the X-ray emission from the two brighter sources and the tail extracting the corresponding spectra from the EPIC-MOS1 data in obs. ID 0152570101 (EPIC-MOS2 data could not be used for the spectral analysis as in this camera the sources were located close to the gap between two different CCDs). The extraction

³ See also http://xmm.esac.esa.int/sas/current/documentation/threads/PN_spectrum_thread.shtml.

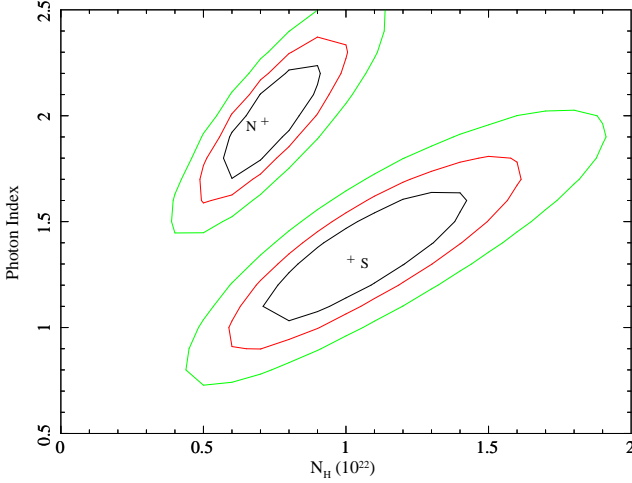


Fig. 4. Contour plot of the absorption column density (N_H) and power law photon index (Γ) derived from the EPIC-MOS1 data for sources N and S in observation ID. 0152570101. The contours correspond to 68%, 90% and 99% confidence levels.

regions (shown in Fig. 3) were chosen in order to maximize the S/N and to minimize the reciprocal contamination. To take into account the background contribution, we selected a circular source-free region of radius 2 arcmin located in the same CCD as IGR J11014-6103 and at approximately the same distance from the central SNR. We also checked that the results presented in this paper would not be affected by different (reasonable) choices of the background region. Given the relatively low number of counts, all the spectra were grouped in order to have at least 5 photons for each energy bin and fit with an absorbed power law model using C-statistics (Cash 1979, ; we used XSPEC v.12). We checked that similar results (to within the uncertainties) would have been obtained by grouping the spectra with 25 photons per energy bin and using χ^2 statistics. The results of the fits are summarized in Table 2. Here we also report the best-fit parameters obtained from the spectral analysis of the entire region (dashed ellipse in Fig. 3). We found marginal evidence for a difference between the power law photon index of sources N and S, and show in Fig. 4 the most relevant contour plots derived from the spectral fits. The spectrum extracted from the tail provided only poor constraints on the properties of its X-ray emission. A similar analysis carried out on the EPIC-MOS and EPIC-pn data of the observation ID. 0111210201 did not reveal any significant variation of the estimated spectral parameters and fluxes from the three regions.

In order to compare the fluxes estimated with *XMM-Newton* and those reported for IGR J11014-6103 in the 4th IBIS/ISGRI catalog (see Sect. 1), we performed a simultaneous fit of the MOS 1 (ID. 0152570101) spectrum from the entire source (dashed ellipse in Fig. 3) and the IBIS/ISGRI spectrum of IGR J11014-6103 obtained from the HEAVENS web-tool. The two spectra could be reasonably well fit using an absorbed power law model, with spectral parameters compatible with those determined previously using only the *XMM-Newton* data (best-fit values reported in the last line of table 2). We obtained $N_H = 0.6 \pm 0.2$, $\Gamma = 1.5 \pm 0.2$ ($\chi^2/\text{d.o.f.} = 0.8/74$) and $C = 1.7^{+1.1}_{-0.6}$. Here, C is the normalization constant introduced to take into account both the intercalibration between the EPIC-MOS1 and IBIS/ISGRI, and any possible flux change of compact emission regions between the different observations. We considered EPIC-MOS1 as reference detector, therefore the constant is applied to the

Table 2. Results of the spectral fit parameters obtained from *XMM-Newton* observation ID. 0152570101. All spectra were fit using an absorbed power law model (photon index Γ). The absorption column densities (N_H) and fluxes are in units of 10^{22} cm^{-2} and $10^{-13} \text{ erg cm}^{-2} \text{ s}^{-1}$, respectively. We also report the estimate of the X-ray flux in the 0.2-2.4 keV energy band ($F_{0.2-2.4 \text{ keV}}$), in order to have an easier comparison with the results obtained from *ROSAT*/HRI observations (see Sect. 2.3). Uncertainties are at 90% c.l. on the spectral parameters and 68% c.l. on the fluxes.

	N_H	Γ	$F_{2-10 \text{ keV}}$	$F_{0.2-2.4 \text{ keV}}$	C-stat/d.o.f.
N	0.7 ± 0.2	2.0 ± 0.3	$3.7^{+0.6}_{-1.1}$	$1.2^{+0.2}_{-0.5}$	68.2/68
S	1.0 ± 0.4	1.3 ± 0.4	$6.2^{+0.9}_{-2.6}$	$0.8^{+0.2}_{-0.4}$	73.3/62
Tail	$1.3^{+0.7}_{-0.8}$	$2.2^{+0.7}_{-0.8}$	$1.9^{+0.3}_{-1.0}$	$0.5^{+0.2}_{-0.3}$	31.1/21
Total	0.7 ± 0.1	1.6 ± 0.15	$17^{+1.2}_{-1.4}$	$3.9^{+0.3}_{-0.5}$	68.60/85

ISGRI spectrum. We noticed that fixing $C=1$ would not significantly change the results of the fit. The estimated 2-10 keV, 20-40 keV, and 40-80 keV X-ray fluxes of the sources were $(1.9 \pm 0.2) \times 10^{-12} \text{ erg cm}^{-2} \text{ s}^{-1}$, $(3.1^{+0.2}_{-0.3}) \times 10^{-12} \text{ erg cm}^{-2} \text{ s}^{-1}$, and $(4.8^{+0.4}_{-0.6}) \times 10^{-12} \text{ erg cm}^{-2} \text{ s}^{-1}$, respectively. These are fully compatible with those reported by Bird et al. (2010), i.e. $(3.0 \pm 0.8) \times 10^{-12}$ and $(5.6 \pm 2) \times 10^{-12} \text{ erg cm}^{-2} \text{ s}^{-1}$ in the 20-40 keV and 40-100 keV band respectively, see Sect. 1. The unfolded MOS1+ISGRI spectrum of IGR J11014-6103 is shown in Fig. 5. A simultaneous MOS1+ISGRI spectral analysis was carried out also using the EPIC spectra of source S alone (without including the tail and source N). This source indeed seems to have a harder spectrum and higher estimated flux in the 2-10 keV band with respect to source N and the tail. No significant differences in the three spectral parameters have been measured, except for a marginal hint of an increase of the intercalibration constant needed in the fit.

We also searched in the EPIC data for indications of variability for sources N and S on time scales of seconds to hours, but did not spot any relevant feature. We paid particular attention in searching for coherent pulsations. We used the PN data for the short observation (ID. 0111210201) and decided to analyze sources N and S jointly, to maximize the number of source photons. Cutting out source S for an analysis of source N (and vice versa) would result in a too high loss of source photons for a detailed timing analysis, respectively. The total number of photons obtained for both sources together was 693. By adopting an epoch-folding technique with 16 phase bins, we determined an upper limit on the pulsed fraction for a sinusoidal signal of 56% (at 90% c.l.) in the 0.002 to 6.8 Hz frequency range (we followed the approach of Leahy et al. 1983). In the long observation (ID. 0152570101) we could use only the data of MOS1 (1275 photons) and MOS2 (2087 photons), and explored therefore the frequency range 0.001–0.2 Hz: the upper limits on the pulsed fraction are 44% and 33% (at 90% c.l.) respectively.

2.3. ROSAT

We retrieved all available *ROSAT* (Truemper 1982) data in the direction of IGR J11014-6103 from the HEASARC archive. The FOV around IGR J11014-6103 was observed with the HRI (Pfeffermann et al. 1987) on-board *ROSAT* on several occasions (observations ID. RH500445A01, RH500340N00, RH500445N00, RH900619A01, and RH900619N00). Among

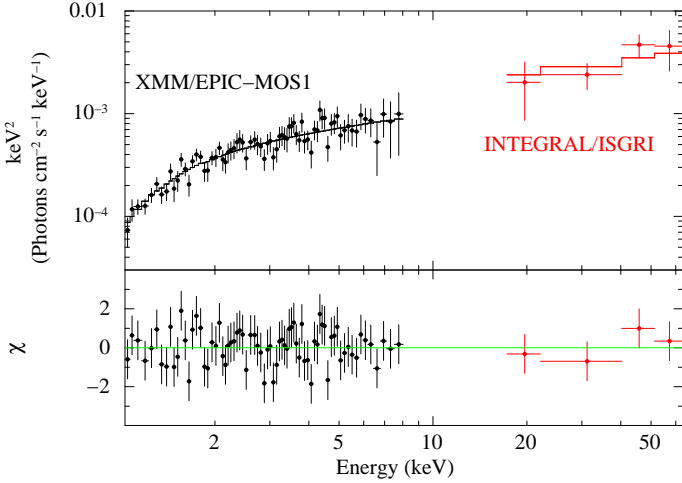


Fig. 5. Unfolded *XMM-Newton* and IBIS/ISGRI spectrum of IGR J11014-6103. We fitted both spectra with a single absorbed power law model (solid line). In the bottom panel we show the residuals from this fit.

these, observation ID. RH500445A01 was characterized by the longest available exposure time (46 ks) and was performed on 1997 June 28. We show in Fig. 6 the HRI image (5'' resolution, 0.2-2.4 keV). Within the *INTEGRAL* error circle of IGR J11014-6103 a single point-like source is detected. This source was already classified in the HRI catalog as 1RXH J110146.1-610121 (Voges et al. 1999). The best determined source position is at $RA=165.442$ deg and $Dec=-61.022$ deg. The nominal positional accuracy of the HRI is of order 10'' (Predehl & Prieto 2001) and thus the *ROSAT* position is consistent with that of the source revealed with *Swift* and with source N detected with *XMM-Newton*. Given the limited spatial resolution, sensitivity and energy coverage of the HRI with respect to the EPIC cameras, it is not surprising that the closeby source S and the tail are not detected in this case (source S is also fainter than source N in the *ROSAT* energy band, see Table 2). We suggest that, as for the case of *Swift*/XRT, the *ROSAT* source is indeed a blend of sources N and S. The estimated count rate of 1RXH J110146.1-610121 in the HRI energy band (0.2-2.4 keV) is 0.0038 ± 0.0004 cts/s. This would convert into an X-ray flux of $(9 \pm 1) \times 10^{-13}$ erg cm $^{-2}$ s $^{-1}$ (2-10 keV) if an absorbed power law spectral model with $N_H = 0.7 \times 10^{22}$ cm $^{-2}$ and $\Gamma = 1.6$ is used (see Sect. 2.2). The flux of the *ROSAT* source is thus qualitatively in agreement with that of sources N and S estimated from *XMM-Newton* data.

We noted that the FOV around IGR J11014-6103 was observed also with the PSPC on-board *ROSAT* on two occasions, on 1993 July 23 (observation ID. RP500307N00) and on 1994 July 5 (observation ID. RP500307A01). However, in these two cases the relative low exposure time (~ 2 ks) and the off-set position of the source with respect to the instrument aim-point, did not result in a clear detection of the source. We thus do not discuss these data in more detail.

2.4. ASCA

In the HEASARC archive we found two observations carried out with the GIS telescope (Ohashi et al. 1996) on-board ASCA (Tanaka et al. 1994) which included the region around IGR J11014-6103 in their FOV. The first of these observations, ID. 51021000, was performed on 1994 March 1 with a total ex-

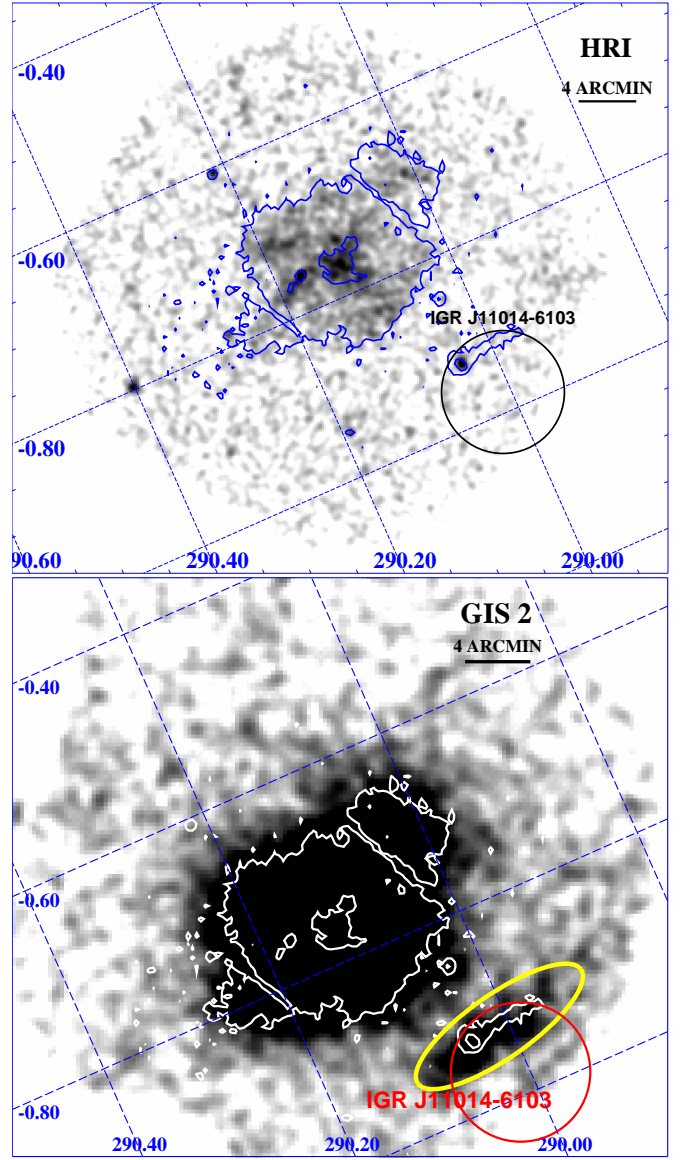


Fig. 6. *Top:* *ROSAT*/HRI FOV around IGR J11014-6103 (observation ID. RH500445A01). The image is in the 0.2-2.4 keV energy band with a resolution of 5'' (see Sect. 2.3). We overplot on this image the *XMM-Newton* contour levels (in blue) determined from the EPIC-MOS1 data in observation ID. 0152570101 (see also Fig. 1). The black circle represents the *INTEGRAL* position of IGR J11014-6103. The bright extended emission in the center of the FOV is SNR MSH 11-61A. *Bottom:* *ASCA*/GIS2 FOV around IGR J11014-6103 (observation ID. 51021000). The image is in the 0.5-10 keV energy band. Extended emission is clearly visible in the bottom right side of the detector, below SNR MSH 11-61A. We overplot on this image the *XMM-Newton* contours (in white), the *INTEGRAL* error circle of IGR J11014-6103 (red circle), and the extraction region adopted for the GIS spectral analysis (yellow ellipse).

posure time of 43.4 ks. The second observation, ID. 51021010, lasted for 40.5 ks and was carried out about 10 months later, on 1995 January 16. Both these observations were aimed at the SNR MSH 11-61A and did not cover entirely the *INTEGRAL* error circle around the position of IGR J11014-6103. However, the extended emitting region already identified with *XMM-Newton* is clearly detected in the GIS images (see Fig. 6). In comparison

with the HRI camera on-board *ROSAT*, the GIS has a broader energy coverage (0.5-10 keV) and a larger sensitivity, but a significantly worse spatial resolution (the GIS PSF is ~ 1 arcmin and strongly dependent on energy, Tanaka et al. 1994). It is thus not surprising that the GIS is not able to distinguish the two sources (N and S) detected with *XMM-Newton* and *ROSAT*, but can reveal the presence of the diffuse emission around them.

We analyzed GIS2 and GIS3 data following standard procedures and the latest available calibration files (see e.g. Pavan et al. 2011, and references therein). Source spectra in the two observations were extracted using the elliptical region shown in Fig. 6. Given the presence of the nearby SNR MSH 11-61A, we extracted the background spectra from different regions located at the same radial distances of IGR J11014-6103 from MSH 11-61A. Even though the S/N of the data was relatively poor, the GIS spectra could be reasonably well fit using an absorbed power law model. From the GIS2 data in observation 51021000, we measured $\Gamma = 1.6 \pm 0.3$ and estimated a 2-10 keV X-ray flux of $(2.1^{+0.2}_{-0.4}) \times 10^{-12}$ erg cm $^{-2}$ s $^{-1}$ ($\chi^2_{\text{red}}/\text{d.o.f.} = 0.7/21$). These values are compatible (to within the errors) with those inferred from the *XMM-Newton* data. From observation 51021010, we obtained $\Gamma = 1.2 \pm 0.5$ and $F_{2-10 \text{ keV}} = (2.1^{+0.3}_{-1.2}) \times 10^{-12}$ erg cm $^{-2}$ s $^{-1}$ ($\chi^2_{\text{red}}/\text{d.o.f.} = 0.9/16$). In both cases we fixed the absorption column density to the best value measured from *XMM-Newton*. Compatible results (to within the uncertainties) were obtained from the GIS3 data.

2.5. Einstein

The region around IGR J11014-6103 was observed also with the *Einstein*/IPC detector (0.2-4.5 keV, Giacconi et al. 1979) on 1980 August 12 with an exposure time ~ 11 ks. A visual inspection of the *Einstein*/IPC image revealed a source (2E 2383) spatially coincident with sources N and S and a marginal evidence for an extended tail similar to that observed in *XMM-Newton*. The best position of 2E 2383 is reported in the 2E catalog at RA = 11^h : 01^m : 47.5^s, Dec = -61°:01':22" (related uncertainty 39", see Fig.1; Harris et al. 1994). The source count rate was 0.011 ± 0.002 cts/s, which correspond to $(9 \pm 2) \times 10^{-13}$ erg cm $^{-2}$ s $^{-1}$ (assuming a column density $N_H = 0.7 \times 10^{22}$ cm $^{-2}$ and a power law spectrum with slope $\Gamma = 1.6$, see Sect. 2.2). This flux is compatible with the one measured with *XMM-Newton*.

3. Counterparts to IGR J11014-6103

In this section we take advantage of the improved positions for the three emitting regions comprised in the *INTEGRAL* error circle around IGR J11014-6103 to search for the corresponding counterparts in the optical, infra-red, and radio domain. In Sect. 3.3, we also report on a possible γ -ray detection.

3.1. Optical/IR data

We used publicly available optical and near infra-red images from STSCI-DSS, and 2MASS surveys. Potential counterparts to sources N and S are shown in Fig. 7. For source N, we did not find any obvious counterpart in the optical domain. The closest catalogued USNO-A2.0 sources are located more than $\sim 7''$ away from the best determined EPIC-MOS1 position of the source. The nearest classified object in the USNO-B1.0 catalog is J0289-0254424 (R1=10.89, B2=15.97), located at RA=165.4471 deg, Dec=-61.0221 deg. In the infra-red domain,

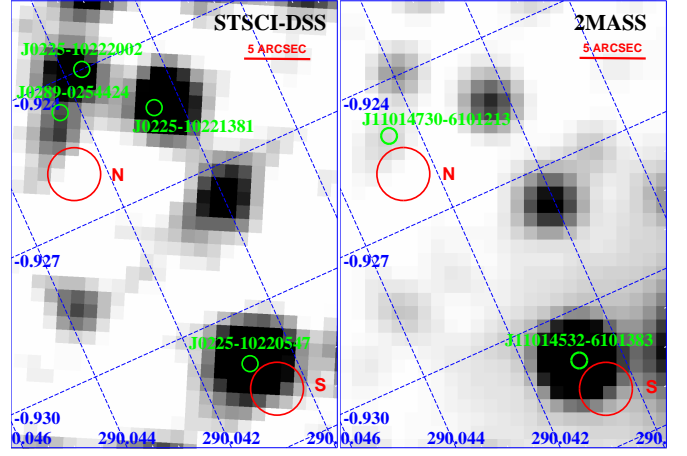


Fig. 7. Search for optical and infra-red counterparts to the sources N and S. *Left:* STSCI-DSS image. We overplot the position of sources N and S (radius equal to the position accuracy, 2") as determined from the EPIC-MOS1 observation, and the most likely optical counterpart from the USNO-A2.0 and USNO-B1.0 catalogs (green circles, with radius 0.6"). *Right:* 2MASS image. The position of sources N and S is indicated as above. We marked the location of the potential infra-red counterparts retrieved from the 2MASS catalog (green circles, with radius 0.6").

the closest catalogued source is the 2MASS object J11014730-6101213 located at RA=165.447122 deg, Dec=-61.022602 deg. This object is reported in the catalog with J=15.95, H=15.54, K=15.46. For source S, the closest catalogued source in the optical domain (USNO-A2.0 catalog) is J0225-10220547. This is located at RA=165.438870 deg, Dec=-61.027375 deg and is characterized by B=16.5 and R=13.0. In the infra-red domain, the closest object from the 2MASS catalog to the position of source S is J11014532-6101383, located at RA=165.438860 deg, Dec=-61.027306 deg and characterized by J=11.16, H=10.19, K=9.89.

3.2. Radio data

To search for radio counterparts to IGR J11014-6103, we used data from the MGPS-2 archive. The MGPS-2 is a high-resolution and large-scale survey of the galactic plane carried out with the Molonglo Observatory Synthesis Telescope (MOST) at a frequency of 843 MHz (Murphy et al. 2007). The MGPS-2 image covering the field around IGR J11014-6103 is shown in Fig. 8. We noticed from this figure the presence of a relatively bright radio source, J110149-610104, positionally consistent with sources N and S. The radio source is reported in the MGPS catalog as "compact", being its dimensions comparable to the convoluted beam of the survey. The best determined position of J110149-610104 is RA=(165.4559 \pm 0.0017) deg, Dec=(-61.0178 \pm 0.0017) deg. The associated flux at 843 MHz is 24.2 \pm 4.8 mJy (corresponding to $(2.04 \pm 0.40) \times 10^{-16}$ erg cm $^{-2}$ s $^{-1}$).

3.3. γ -ray data

We also noticed the presence of an *EGRET* source, 3EG J1102-6103, which might be related with IGR J11014-6103. In the latest available *EGRET* catalog, the best determined position of 3EG J1102-6103 is at RA=165.60 deg, Dec=-61.05 deg, with

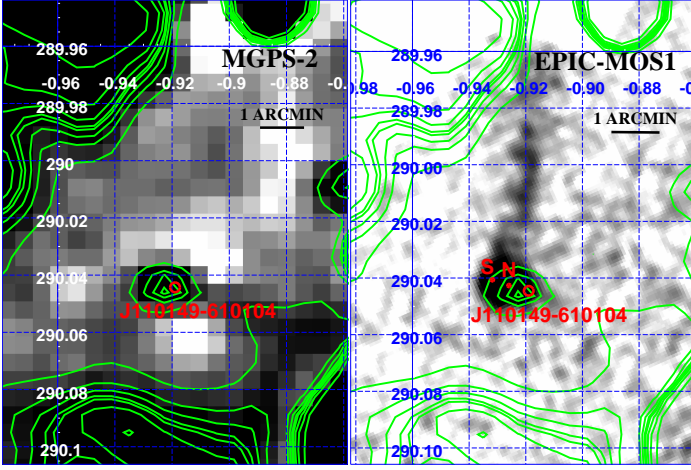


Fig. 8. *Left:* radio image (and contours) at 843 MHz around the position of IGR J11014-6103 retrieved from the MGPS-2 archive. We mark in red the position of the source MGPS2J110149-610104. *Right:* EPIC-MOS1 image from observation ID. 0152570101. We overplot on the image the radio contours derived from the MGPS-2 data in green and marked in red the position of the radio source J110149-610104 and the two *XMM-Newton* sources N and S.

an associated uncertainty of 0.6 deg. The error circle around 3EG J1102-6103 would thus be compatible with the position of IGR J11014-6103, as determined before. At present, however, we are unable to confirm this association due to the presence of other possible counterparts located within the *EGRET* error circle of 3EG J1102-6103. Among these, there are the SNR MSH 11-61A and the young energetic pulsar PSR J1105-6107 (Kaspi et al. 1997).

In the *Fermi*/LAT catalog we did not find any source positionally coincident with IGR J11014-6103. We did not attempt an estimate of an upper limit on the source flux from the *Fermi* data. The latter calculation would indeed depend crucially on the properties of the still relatively poorly known high energy Galactic background in such a highly crowded region.

4. Discussion and conclusions

In this paper we analyzed all publicly available X-ray observations carried out in direction of the unidentified source IGR J11014-6103 with *Swift*, *XMM-Newton*, *ROSAT*, *ASCA* and *Einstein*. The entire *INTEGRAL* error circle around IGR J11014-6103 has been covered in the soft (1-10 keV) X-ray energy band with *Swift* and *ROSAT*. The analysis of these data led to the detection of a single X-ray source inside the error circle given by *INTEGRAL* (see also Malizia et al. 2011). However, the deepest observations of the region around IGR J11014-6103, performed with the EPIC cameras on-board *XMM-Newton*, revealed that the source detected with *Swift*/XRT and *ROSAT* is likely a blend of two distinct objects: a point-like source and an 8.1 arcsec extended object. The same observations revealed also the presence of a cometary-like tail (~ 4 arcmin) extending from the two sources, and comprised within the *INTEGRAL* error circle around IGR J11014-6103. The X-ray spectra of the three objects displayed only marginally significant differences (see Table 2 and Fig. 4).

The *ROSAT*/HRI and *ASCA*/GIS observations of the same region were unable to disentangle the three emitting components. This can be ascribed to the narrower energy range coverage of

the former instrument and the lower spatial resolution of the telescopes on board *ASCA* and *ROSAT* with respect to the EPIC cameras (see fluxes in the 0.2-2.4 keV band in Table 2 and Sect. 2.3, 2.4). In all cases, we showed that the X-ray emitting properties of the entire region comprised in the *INTEGRAL* error circle of IGR J11014-6103 were in agreement among all the available instruments. In Sect. 2.2, we also showed that the joint *XMM-Newton*+*INTEGRAL* spectrum could be reasonably well described using a single absorbed power law model, with a normalization constant between the two instruments $\simeq 1$. All these results suggest that IGR J11014-6103 is a persistent X-ray emitter that displayed in the past ~ 31 years only marginal variations (if any) in the 0.3-100 keV energy band.

The improved X-ray positions of sources N and S permitted also to search for their possible optical and infra-red counterparts. The closest catalogued 2MASS, USNO-A2.0, and USNO B1.0 objects to sources N and S lie just outside the 90% c.l. error circle determined with *XMM-Newton*; further observations with the ACIS telescope on-board *Chandra* are therefore needed to reduce the likelihood of a chance coincidence. We found a possible radio counterpart close to sources N and S. The radio contours derived from the publicly available MGPS-2 data match reasonably well with those of the X-ray emission detected with *XMM-Newton* around sources N and S. The presence of an *EGRET* source, 3EG J1102-6103, positionally coincident with IGR J11014-6103 was also reported.

Being IGR J11014-6103 located only 11 arcmin apart from the nearby SNR MSH 11-61A, we first considered the possibility that the X-ray emission coming from the unidentified *INTEGRAL* source was related to the SNR. However in none of the investigated wavelengths (X-ray, radio, optical, NIR) we could clearly identify the presence of emitting structures located between MSH 11-61A and IGR J11014-6103 which could have favored such an association (see also Rosado et al. 1996).

As an alternative and perhaps more viable hypothesis, we considered that the morphology and emission properties of the 4 arcmin extended X-ray tail in IGR J11014-6103 might resemble the elongated features observed in the case of PSR B2224+65 (“the Guitar” nebula, Hui & Becker 2007) and PSR J0357+3205 (De Luca et al. 2011). In both cases a pulsar (PSR) has been firmly detected at one end of the elongated structures, and the cometary-like tails have been tentatively explained under the “bow-shock pulsar wind nebulae” (bsPWN) scenario. These elongated cometary-like objects form when a pulsar escapes from the associated supernova remnant and moves with a very high velocity through the interstellar medium (typically hundreds of km/s, i.e. orders of magnitude higher than the velocities of the cold and warm components of the interstellar medium, see e.g. Roberts et al. 2005, and references therein). Close to the pulsar, the relativistic wind of the compact object usually gives rise to a sub-luminous cavity in X-rays surrounded by a termination shock. In this region, particles are thermalized and accelerated, thus producing a conspicuous X-ray and radio emission (through synchrotron processes due to the interaction with the local magnetic field). As the pulsar is moving, a bow shock is formed in front of it and the flow of material advects the emitting particles back along the direction of motion, leading to the formation of an elongated cometary structure (see e.g. Gaensler & Slane 2006, for a detailed discussion). In a few cases, deep X-ray observations with the ACIS telescope on-board *Chandra* permitted to clearly disentangle the different contributions to the total X-ray and radio emission produced by

the structures around a bsPWN (see e.g. the case of the PWN G359.23-0.82; Gaensler et al. 2004).

If the structures detected in IGR J11014-6103 are indeed originating from the pulsar wind, the X-ray tail can be interpreted as being due to relic electrons spread along the direction of motion of the PSR. Source N, extended in X-rays and closer to the peak of the radio emission, would represent, according to this interpretation, the compact PWN (with possible contribution coming also from the bow-shock). The detection of a radio source located close to source N would support this scenario, as radio synchrotron emission is expected from particles accelerated at the termination shock; see the cases of, e.g. PSRs B1853+01 (Frail et al. 1996; Petre et al. 2002), B1957+20 (Stappers et al. 2003), B1757-24 (Frail & Kulkarni 1991; Kaspi et al. 2001).

While the association between the extended source N and the “tail” seems morphologically plausible, the association of source S to this region is less straightforward.

In case source S is not physically related to the X-ray tail, it might just by chance be located along the line of sight to the extended structure. The pulsar responsible for the formation of the compact and relic PWNs, might, in this case, be unresolved and comprised in the emission detected from source N.

In case, instead, that source S, the point-like source, is physically connected to the PWN, it would be reasonable to associate it to the PSR generating the X-ray structures. Under this scenario the misalignment between the direction of the 4 arcmin tail and the axis between sources N and S would imply a significant tilt between the proper motion of the PSR and the position of the compact PWN. A similar misalignment, however, was already observed in e.g. PSR B2224+65, and ascribed to the strong interaction between the fast-moving pulsar and its dense surrounding environment (Hui & Becker 2007). Indeed, as for the case of PSR B2224+65, also the environment around MSH 11-61A and IGR J11014-6103 was found to be a complex and dense region, characterized by the presence of several background and foreground molecular clouds (Filipovic et al. 2005, and references therein).

Following the joint XMM+ISGRI spectral analysis (see Sect. 2.2), we conservatively assume that both sources N and S contribute to the ISGRI emission (the tail component has indeed a much lower flux). Spectral properties (hardness and flux stability) similar to those observed in the present case (see Fig. 5) have already been measured in, e.g. AX J1838-0655. This source is a young ($\tau_c \equiv P/2\dot{P} = 23$ kyr) pulsar, surrounded by a PWN (Gotthelf & Halpern 2008). The best-fit power law slope in the 2-100 keV was measured at $\Gamma = 1.5 \pm 0.2$ (Malizia et al. 2005). We note however that also the highly-magnetized neutron stars (“magnetars”, for a review see e.g. Mereghetti 2008) share similar spectral properties. SGR 1806-20, for example, showed a power law slope $\Gamma = 1.6 - 2.0$ in the range 1-100 keV (Esposito et al. 2007). As the 1-10 keV spectra of magnetars are usually (phenomenologically) modelled with a combined black body+power law (BB+PL) model (Mereghetti 2008), the lack of the BB component in the XMM-Newton spectrum might be an issue for this interpretation. We therefore estimated for source S (i.e. the component showing the higher 2-10 keV flux) the contribution of an eventual black body spectral component. We used a temperature $kT = 0.5$, in agreement with the one measured for SGR 1806-20 (Esposito et al. 2007) and for magnetars in general. Due to the relative low S/N, we could only obtain a poorly constrained upper limit on the ratio between the fluxes of the BB and PL components $F_{BB}/F_{PL} < 0.1$. This would be compatible with the value measured in the case of

SGR 1806-20 ($F_{BB}/F_{PL} = 0.03$, Esposito et al. 2007). The present data therefore do not argue against a magnetar hypothesis. We note also that a PWN associated to a magnetar has already been observed, e.g. in the case of AXP 1E1547.0-5408 (Vink & Bamba 2009).

Further observations with an X-ray telescope characterized by a finer spatial resolution (i.e. the ACIS on-board *Chandra*) and increased spectral and timing statistics are required to solve the issues above and firmly establish the real nature of IGR J11014-6103. In case these observations will confirm that IGR J11014-6103 is a newly discovered PWN generated by a high-velocity PSR, this would be the first detection with *INTEGRAL* of one of these systems (to the best of our knowledge).

Acknowledgements. This work made use of data obtained from the High Energy Astrophysics Science Archive Research Center (HEASARC), provided by NASA’s Goddard Space Flight Center. We thank an anonymous referee for useful comments.

References

- Bird, A. J., Bazzano, A., Bassani, L., et al. 2010, *ApJS*, 186, 1
- Bozzo, E., Giunta, A., Stella, L., et al. 2009, *A&A*, 502, 21
- Burrows, D. N., Hill, J. E., Nousek, J. A., et al. 2005, *Space Sci. Rev.*, 120, 165
- Cash, W. 1979, *ApJ*, 228, 939
- Chaty, S., Zurita Heras, J. A., & Bodaghee, A. 2010, *ArXiv:astro-ph/1012.2318*
- De Luca, A., Marelli, M., Mignani, R., et al. 2011, *Arxiv preprint arXiv:1102.3278*, *The Astrophysical Journal*, 35
- Esposito, P., Mereghetti, S., Tiengo, A., et al. 2007, *A&A*, 476, 321
- Filipovic, M., Payne, J., & Jones, P. 2005, *Serbian Astronomical Journal*, 170, 47
- Frail, D. A., Giacani, E. B., Goss, W. M., & Dubner, G. 1996, *ApJL*, 464, L165
- Frail, D. A. & Kulkarni, S. R. 1991, *Nature*, 352, 785
- Gaensler, B. & Slane, P. 2006, *ARA&A*, 44, 17
- Gaensler, B., Swaluw, E., Camilo, F., et al. 2004, *ApJ*, 616, 383
- Gehrels, N., Chincarini, G., Giommi, P., et al. 2004, *ApJ*, 611, 1005
- Giacconi, R., Branduardi, G., Briel, U., et al. 1979, *ApJ*, 230, 540
- Gotthelf, E. V. & Halpern, J. P. 2008, *ApJ*, 681, 515
- Harris, D., Forman, W., Gioia, I., et al. 1994, *EINSTEIN Observatory catalog of IPC X-ray sources*, *SAO HEAD CD-ROM Series I (Einstein)*
- Hui, C. & Becker, W. 2007, *A&A*, 467, 1209
- Kaspi, V. M., Bailes, M., Manchester, R. N., et al. 1997, *ApJ*, 485, 820
- Kaspi, V. M., Gotthelf, E. V., Gaensler, B. M., & Lyutikov, M. 2001, *ApJL*, 562, L163
- Leahy, D. A., Darbro, W., Elsner, R. F., et al. 1983, *ApJ*, 266, 160
- Malizia, A., Bassani, L., Stephen, J. B., et al. 2005, *ApJ*, 630, L157
- Malizia, A., Landi, R., Bassani, L., et al. 2011, *The Astronomer’s Telegram*, 3290, 1
- Mereghetti, S. 2008, *A&Ar*, 15, 225
- Murphy, T., Mauch, T., Green, A., et al. 2007, *MNRAS*, 382, 382
- Ohashi, T., Ebisawa, K., Fukazawa, Y., et al. 1996, *PASJ*, 48, 157
- Pavan, L., Bozzo, E., Ferrigno, C., et al. 2011, *A&A*, 526, A122
- Petre, R., Kuntz, K. D., & Shelton, R. L. 2002, *ApJ*, 579, 404
- Pfeffermann, E., Briel, U. G., Hippmann, H., et al. 1987, in *Presented at the Society of Photo-Optical Instrumentation Engineers (SPIE) Conference*, Vol. 733, *Society of Photo-Optical Instrumentation Engineers (SPIE) Conference Series*, ed. E.-E. Koch & G. Schmahl, 519
- Predehl, P. & Prieto, A. 2001, *ArXiv:astro-ph/0109542*
- Roberts, M., Brogan, C., Gaensler, B., et al. 2005, *Astrophysics and Space Science*, 297, 93
- Rosado, M., Ambrocio-Cruz, P., Le Coarer, E., & Marcelin, M. 1996, *A&A*, 315, 243
- Stappers, B. W., Gaensler, B. M., Kaspi, V. M., van der Klis, M., & Lewin, W. H. G. 2003, *Science*, 299, 1372
- Tanaka, Y., Inoue, H., & Holt, S. S. 1994, *PASJ*, 46, L37
- Truemper, J. 1982, *Advances in Space Research*, 2, 241
- Ubertini, P., Lebrun, F., Di Cocco, G., et al. 2003, *A&A*, 411, L131
- Vink, J. & Bamba, A. 2009, *ApJ*, 707, L148
- Voges, W., Aschenbach, B., Boller, T., et al. 1999, *A&A*, 349, 389
- Walter, R., Röhlf, R., Meharga, M., et al. 2010, *PoS(INTEGRAL 2010)*, 162
- Watson, M. G., Schröder, A. C., Fyfe, D., et al. 2009, *A&A*, 493, 339
- Winkler, C., Courvoisier, T., Di Cocco, G., et al. 2003, *A&A*, 411, L1